Journal of Fluids and Structures (1998) **12,** 353–365

ON THE OPTIMAL DESIGN OF PIPES CONVEYING FLUID

D. BORGLUND

Department of Aeronautics, Royal Institute of Technology
S-100 44 Stockholm, Sweden

(Received 17 April 1997 and in revised form 14 November 1997)

The stability and optimal design of a beam subject to forces induced by fluid flow through attached pipes is investigated. The structure is assumed to have the same dynamics as a fluid-conveying pipe, and the dynamic stability is analysed using a finite element formulation of the linear equation of motion. The optimal design problem of minimizing the structural mass at fixed critical flow speed is solved. The numerical results are compared to experiments with satisfactory agreement, provided that the lower bounds of the beam dimensions are properly chosen. The influence of structural damping on the critical flow speed is significant, and is found to be strongly design-dependent.

1. INTRODUCTION

The stability of a structure subject to nonconservative fluid-dynamic forces can often be analysed using the linear equations of motion in the form

$$\mathbf{M}\ddot{\mathbf{w}} + \mathbf{D}\dot{\mathbf{w}} + \mathbf{K}\mathbf{w} - q\mathbf{Q}\mathbf{w} = \mathbf{0}, \tag{1}$$

where the vector $\mathbf{w}$ denotes the nodal displacements of the structural finite element model, $\mathbf{M}$ the consistent mass matrix, $\mathbf{K}$ the stiffness matrix, $\mathbf{D}$ the damping matrix and $\mathbf{Q}$ the external (circulatory) force matrix. A dot denotes differentiation with respect to time t. The scalar parameter q denotes the magnitude of the external forces, for example a fluid dynamic pressure (Dowell *et al.* 1989) or the magnitude of a rocket thrust (Sugiyama *et al.* 1995).

A difficulty with the optimal design of structures subject to nonconservative forces is that the optimal design may be very sensitive to imperfections. In practice, this means that small perturbations may cause significant reductions in performance. Consequently, experimental verification of the theoretically predicted improvements is very important.

In order to increase the understanding of the problem of optimal design of structures with fluid interaction, analysis of adequate model problems is useful. The linear dynamics of a cantilevered flexible pipe conveying fluid is represented by an equation of motion in the form (1), meaning that there are many similarities between flutter of a fluid conveying pipe and, for example, aircraft structures. The problem of fluid-conveying pipes has attained much interest and many papers on the subject have been published. For a recent review see Paidoussis & Li (1993). The problem of optimal design of fluid-conveying pipes has also been studied in some detail by Langthjem (1996) and Tanaka *et al.* (1993). A related problem is the optimal design of a beam subject to a compressive follower force. An example

0889-9746/98/030353 + 13 $25.00/fl970135

of a recent study of the optimal design of such a beam, known as *Beck's column*, is given in Ringertz (1994).

2. THE MODEL PROBLEM

The system to be studied in the present paper is shown schematically in Figure 1. It is composed of a thin and slender beam with two attached circular tubes, aligned symmetrically on each side. A cantilevered configuration hanging vertically downward is considered. The fluid-dynamic forces due to fluid flow in the tube may cause the structure to become unstable at some critical flow speed.

A theoretical model of a flexible beam with centred flow is assumed to be sufficient, although the present system is more complex. Consequently, the system is assumed to have the same dynamics as a cantilevered pipe, but is considered to be more experimentally feasible for several reasons. For example, static distortion due to initially curved shapes of the tubes (Paidoussis & Li 1993) is reduced, since the tubes are straightened along the beam. Further, the manufacturing of theoretically designed structures is simplified. It is easier to manufacture a beam with a varying width, than a tube with a varying outer radius (Langthjem 1996). It is also easier to attach sensors and actuators to the beam structure.

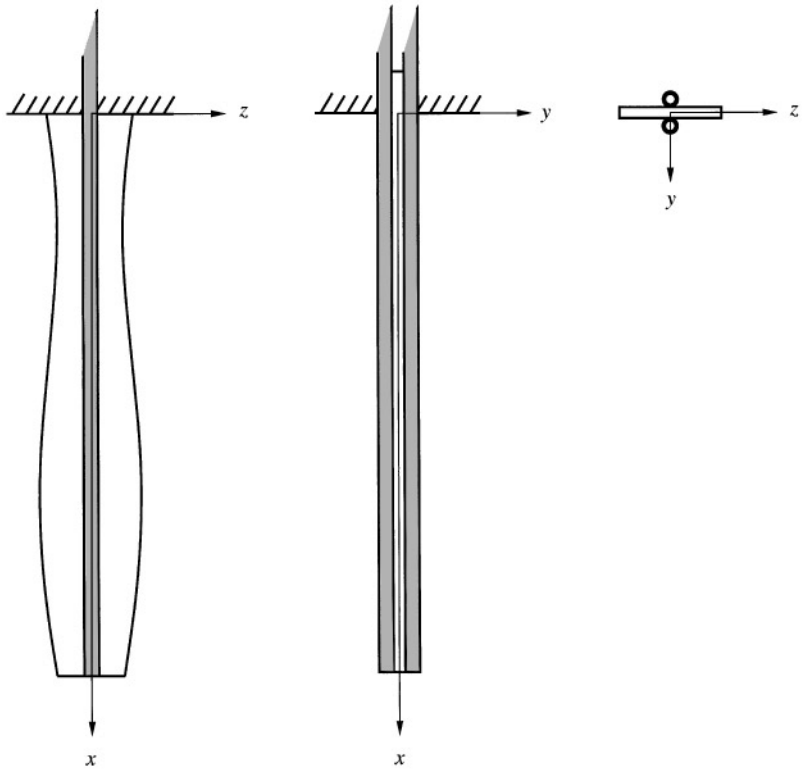

Figure 1. Schematic layout of the model problem.

2.1. Equation of Motion

In the following, the subscripts t and b refer to "tube" and "beam" properties. The beam, with length l, is modelled viscoelastic using a Kelvin–Voigt material type with density ρ_b, Young's modulus E_b and dynamic viscosity coefficient E_b^*. Further, it may have a varying width $w(x)$ but constant thickness h, giving an area-moment of inertia $I_b(x)$ and mass per unit length $m_b(x)$. Using the same material model, the tubes have the corresponding properties ρ_t, E_t and E_t^*, but have a fixed geometry with total area-moment of inertia (with respect to the beam centre axis) I_t and total mass per unit length m_t. The tube conveys a fluid with mass per unit length m_f and flow speed U. Concentrated masses m_i at the positions x_i, $i = 1, \ldots, n_c$, may also be included.

Assuming Euler–Bernoulli beam theory and the plug-flow approximation for the fluid-dynamic forces, one obtains the partial differential equation governing the linear dynamics (Paidoussis 1970),

$$\begin{aligned}(m_l + m_f)\ddot{y} + [(E_b^* I_b + E_t^* I_t)\dot{y}'']'' + 2m_f U\dot{y}' + cw\dot{y} \\ + g\left[(m_l + m_f)y' - \int_x^l (m_l + m_f)\,dx\,dy''\right] + m_f U^2 y'' \\ + [(E_b I_b + E_t I_t)y'']'' = 0,\end{aligned} \tag{2}$$

with boundary conditions

$$\begin{aligned} y = y' = 0 \quad &\text{at } x = 0, \\ (E_b I_b + E_t I_t)y'' + (E_b^* I_b + E_t^* I_t)\dot{y}'' = 0 \quad &\text{at } x = l, \\ [(E_b I_b + E_t I_t)y'' + (E_b^* I_b + E_t^* I_t)\dot{y}'']' = 0 \quad &\text{at } x = l, \end{aligned} \tag{3}$$

for the cantilevered beam. In equations (2) and (3) a dot denotes differentiation with respect to time t and a prime denotes differentiation with respect to location x. The total mass per unit length of the structure is given by

$$m_l(x) = m_b(x) + m_t + \sum_{i=1}^{n_c} m_i \delta(x - x_i), \tag{4}$$

and g denotes the acceleration due to gravity. Concentrated masses are included using the Dirac delta function $\delta(x)$.

The different terms in equation (2) are, in order of appearance, the inertia force, the internal damping force, the Coriolis force, the viscous damping force, the gravity force, the centrifugal force and the flexural restoring force. Linear design-dependent viscous damping is included by assuming that the viscous damping force is proportional to the beam width. Hence, c is the viscous damping coefficient corresponding to this model. Damping normally has a stabilizing effect, but may be destabilizing in nonconservative systems such as this (Paidoussis 1970). Concentrated masses have a destabilizing effect in most cases (Hill & Swanson 1970).

2.2. Numerical Analysis

The equation of motion (2) is discretized using Hermitian finite elements (Langthjem 1996) assuming a symmetric and piecewise linear beam width, giving

$$\mathbf{M}\ddot{\mathbf{w}} + (\mathbf{D} + U\mathbf{C})\dot{\mathbf{w}} + \mathbf{K}\mathbf{w} - U^2\mathbf{Q}\mathbf{w} = \mathbf{0}, \tag{5}$$

where

$$\mathbf{D} = \delta_b \mathbf{K}_b + \delta_t \mathbf{K}_t + c_b \mathbf{M}_b,$$
$$\mathbf{K} = \mathbf{K}_b + \mathbf{K}_t + \mathbf{G}, \tag{6}$$
$$\mathbf{Q} = \mathbf{Q}_c - \mathbf{Q}_n,$$

and the parameters $\delta_t = E_t^*/E_t$, $\delta_b = E_b^*/E_b$ and $c_b = c/\rho_b h$ have been introduced for convenience. The total mass matrix $\mathbf{M}$, the beam mass matrix $\mathbf{M}_b$, the beam and tube stiffness matrices $\mathbf{K}_b$ and $\mathbf{K}_t$, the gravity matrix $\mathbf{G}$ and the conservative load matrix $\mathbf{Q}_c$ are symmetric and positive definite, while the Coriolis (gyroscopic) matrix $\mathbf{C}$ and the nonconservative load matrix $\mathbf{Q}_n$ are nonsymmetric. As before, $\mathbf{w}$ is the vector of nodal displacements and rotations of the finite element model.

Further, the discretized equations of motion are written in state-space form

$$\dot{\mathbf{v}} = \mathbf{A}\mathbf{v}, \tag{7}$$

where

$$\mathbf{v} = \begin{Bmatrix} \mathbf{w} \\ \dot{\mathbf{w}} \end{Bmatrix} \tag{8}$$

and

$$\mathbf{A} = \begin{bmatrix} \mathbf{0} & \mathbf{I} \\ -\mathbf{M}^{-1}(\mathbf{K} - U^2\mathbf{Q}) & -\mathbf{M}^{-1}(\mathbf{D} + U\mathbf{C}) \end{bmatrix}. \tag{9}$$

Solutions of equation (7) are assumed to be of the form

$$\mathbf{v} = \hat{\mathbf{v}} e^{\lambda t}, \tag{10}$$

where $\lambda = \alpha + i\omega$, α being an amplification factor and ω the (circular) flutter frequency. Inserting equation (10) into equation (7) gives the linear eigenvalue problem

$$(\mathbf{A} - \lambda \mathbf{I})\hat{\mathbf{v}} = \mathbf{0}, \tag{11}$$

which is easily solved. Theoretically, the structure is stable for a given flow speed if all n_λ eigenvalues λ have negative real part.

3. EXPERIMENTAL APPROACH

A schematic layout of the experimental set-up is shown in Figure 2. The main components are a water tank (1), a constant flow-rate centrifugal pump (2), a mechanical flow meter (3) and an experimental rig (4) in which the beam structure (5) is mounted. The flow through the beam structure is regulated using a by-pass (6) and two flow control values (7,8).

The experimental equipment was tested at an early stage by reproducing Langthjem's flutter experiments on tubes B and C in Langthjem (1996), using tube material supplied by Langthjem. The experiments matched Langthjem's to within 1%.

3.1. Structural Design and Material Properties

First, a uniform acrylic beam with length $l = 1{\cdot}5$ m, width $w = 0{\cdot}15$ m and average thickness $h = 3{\cdot}12$ mm was considered. The thickness of the acrylic sheets (from which the beams were extracted) was nominally 3·0 mm, but was found to vary slightly. The thickness was taken as

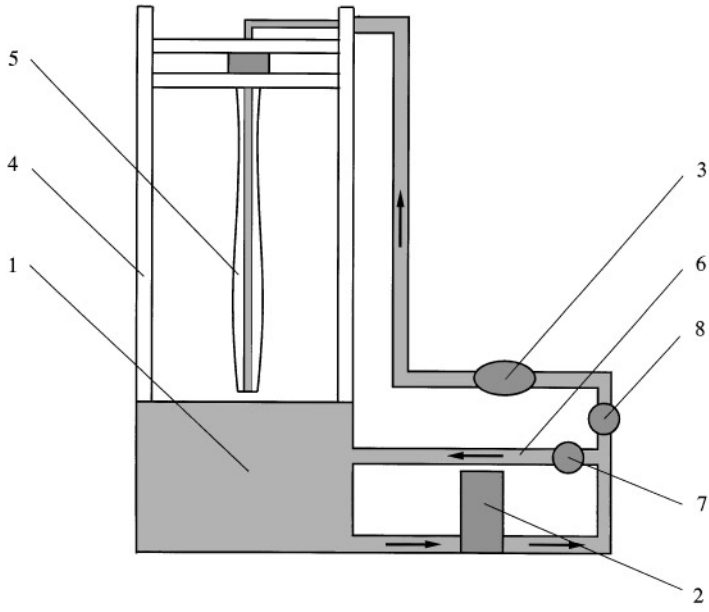

Figure 2. Schematic layout of the experimental set-up.

the average of a series of thickness measurements along the acrylic sheet from which the beam was to be made. Two reinforced silicone rubber tubes with inner and outer radius 8·0 and 14·0 mm were attached to the beam using small cable ties every 0·1 m. Due to the surface properties of the acrylic and rubber, a sufficient adhesion was thus obtained. Further, a removable tip mass, m_c, was fabricated. The tip mass was simply a piece of metal pipe, sliced in such a manner that the centre of gravity coincided with the beam end. Rotary inertia of the mass is neglected.

Measurements of masses and lengths were straightforward. The density of the water was assumed to be $\rho_f = 1000\,\mathrm{kg/m^3}$ and the acceleration of gravity $g = 9{\cdot}81\,\mathrm{m/s^2}$. The elastic material properties of the beam were determined through quasi-static three-point bending tests (Curtis 1988) on test specimens. Accordingly, the elastic properties of the tubes were determined through tensile tests using a clip-gauge. The damping parameters were obtained using a dynamic method (Paidoussis 1970). An outline of the methodology used is given in the next section. The experimentally determined properties used throughout the study, are given in Table 1.

3.2. Determining Material Parameters

If the values $U = 0$ and $m_f = 0$ are used in the equation of motion (2), the problem of a vertical vibrating cantilever is obtained. Estimates of the viscoelastic properties were obtained by matching the logarithmic decrement of the first eigenmode of the cantilever beam to experiments.

In general, both viscous and structural damping are present simultaneously, and their individual contributions to the decay of motion cannot be distinguished. However, the

TABLE 1
Experimentally determined properties

Parameter	Value	Unit
m_c	0·152	kg
ρ_b	1188	kg/m^3
ρ_t	1225	kg/m^3
E_b	$3{\cdot}24 \times 10^9$	N/m^2
E_t	$5{\cdot}43 \times 10^6$	N/m^2
E_b^*	$8{\cdot}54 \times 10^7$	Ns/m^2
E_t^*	$4{\cdot}72 \times 10^5$	Ns/m^2
c	0·235	kg/m^2 s

viscous damping can be estimated independently from the motion of a pendulum with the same geometry as the elastic structure. Using the same model for the viscous damping force as in Section 2.1, Newton's second law yields the (linearized) equation of motion of the pendulum,

$$\int_0^l m_l x^2 \, \mathrm{d}x \, \ddot{\theta} + c \int_0^l w x^2 \, \mathrm{d}x \, \dot{\theta} + g \int_0^l m_l x \, \mathrm{d}x \, \theta = 0, \tag{12}$$

where θ is the angle from the vertical equilibrium position. The solution of equation (12) provides a relation between the logarithmic decrement of the motion and the viscous damping coefficient c. A uniform pendulum with the same dimensions as the beam structure in the previous section was manufactured by replacing the tubes with aluminium pipes. The small amplitude motion of the pendulum was recorded using a low-torque precision potentiometer.

With known viscous damping, the structural damping was found from vibration tests of the elastic structure. First, the viscoelastic properties of the beam were determined independently by removing the tubes in the vibration test, and using the corresponding mass and stiffness distributions in the model. Finally, with known viscous and beam structural damping, the tube structural damping was determined by a vibration test of the complete structure. In the elastic tests the motion was recorded using a strain gauge attached to the beam.

3.3. EXPERIMENTAL PROCEDURE

To simplify the measurements, an automatic control system for the by-pass control valve (see Figure 2) was designed and fabricated. The flow meter provided the possibility of a computerized measurement of the flow speed. A personal computer automatically adjusted the flow speed to a specified value using a simple control law written in the LabVIEW software (Johnson 1994).

Close to the critical speed the flow was increased in small steps, so that possible transients were allowed to settle. The point of instability was determined visually and was defined simply as the lowest velocity resulting in a detectable periodic oscillation of the beam structure. The flutter frequency was estimated by measuring the total time for a large number of periods. It is noted that the frequency is measured after a limit-cycle, determined

by nonlinear forces, has been established. This means that the frequency is measured at a flow speed higher than the critical. If necessary, the flow speed was increased slightly above the critical on purpose, in order to achieve a distinct periodic motion. Consequently, greater emphasis is placed on the prediction of the critical flow speed than on the critical frequency. This is also discussed in Paidoussis (1970). The post-critical behaviour determining the type of Hopf bifurcation was studied in separate tests [see Langthjem (1996)].

3.4. Results

For the uniform beam with the tip mass included, flutter was initiated at the critical flow speed $U_{\text{exp}} = 13{\cdot}8$ m/s. In Table 2 the experiments are compared with numerically obtained results, carried out with 16 finite elements. For comparison with other work on the subject, the results are also presented using Paidoussis' (1970) nondimensional flow speed $u = (m_f/EI)^{1/2}\, Ul$, EI being the total beam-tube structural stiffness. The effect of damping on the critical flow speed is investigated by including the different contributions gradually in the theoretical model. The deviation between numerically predicted and experimentally obtained values is calculated according to the error percentage measure

$$e_U = \frac{|U_{\text{exp}} - U_{\text{pred}}|}{\text{mean}\,(U_{\text{exp}}, U_{\text{pred}})}. \tag{13}$$

It is seen that the inclusion of damping is essential to achieve an accurate prediction of the critical flow speed. The structural damping causes a significant increase of the critical speed, while the viscous damping has little effect. Thus, a satisfying accuracy of the predicted critical flow speed of the uniform beam is obtained, considering that the mechanical flow meter has a specified maximum relative error of $\pm 2\%$.

The experimentally obtained flutter frequency was 1·49 Hz, and the theoretical value is 1·28 Hz. The deviation between these two results is 17%, using the same measure as above. As mentioned in Section 3.3, the frequency was measured at a flow speed slightly higher than the critical, which is a possible reason for the higher frequency obtained in the experiment. The same characteristics were observed in all subsequent tests. For a flow speed slightly lower than the critical, the system was asymptotically stable subject to a strong disturbance, suggesting a supercritical Hopf bifurcation.

Finally, it is noted that the critical flow speed is very sensitive to imperfections in the beam thickness distribution. In this case, a variation in the average thickness of 0·1 mm gives a variation in critical speed of the same magnitude as the observed deviation between theory and experiments.

Table 2
Comparison between predicted and experimentally obtained critical flow speed for the uniform beam

Theoretical model	u_{pred}	u_{exp}	U_{pred} (m/s)	U_{exp} (m/s)	e_U (%)
Damping excluded	4·8	5·7	11·8	13·8	16
Viscous damping	4·9	5·7	11·8	13·8	16
Viscous and tube structural damping	5·2	5·7	12·7	13·8	8·3
Viscous and total structural damping	5·8	5·7	14·2	13·8	2·9

4. OPTIMAL DESIGN

The problem of minimizing the structural mass for a specified critical flow speed U_{cr} will be analysed for a few configurations. This is posed as the nonlinear optimization problem

$$\min_{w_j} m(w_j), \tag{14}$$

$$\mathscr{R}e\,\lambda_i(w_j, U) \leq 0 \quad \text{for all } U \in [0, U_{\mathrm{cr}}], \quad i = 1, \ldots, n_\lambda, \tag{15}$$

$$w_j \geq \underline{w}_j, \quad j = 1, \ldots, n_d, \tag{16}$$

where m is the total structural mass, λ_i the eigenvalues obtained by solving the eigenvalue problem (11) and w_j the design variables. In the present problem, beam nodal widths and concentrated masses are the possible design variables.

The nonlinear programming problem defined by equations (14)–(16) is solved using the method of moving asymptotes (MMA) developed by Svanberg (1993). The MMA method solves the nonlinear programming problem by solving a sequence of approximate convex nonlinear and separable subproblems. Each subproblem is solved by forming the dual function which is maximized subject to bound constraints on the dual variables. The method is locally linearly convergent and cannot be shown to be globally convergent. The method has been proven very useful in a large number of different applications.

The derivatives of the constraint functions (15) are derived as described in Haftka & Adelman (1993). The derivatives of the constraint functions exist provided that the eigenvalues of equation (11) are distinct.

4.1. Optimal Design with Fixed Tip Mass

The first optimal design problem considered is to find the width distribution of the beam with fixed tip mass, such that the structural mass is minimized for a specified critical flow speed. A new uniform design with length $l = 1{\cdot}5$ m, width $w_0 = 0{\cdot}15$ m and average thickness $h = 2{\cdot}80$ mm, shown as Design 1 in Figure 3, was chosen as a reference for the design optimization. Theoretically, this beam has the critical flow speed $U_{\mathrm{pred}} = 12{\cdot}8$ m/s.

The beam geometry was divided into 30 sections of equal length and linearly varying width, giving $n_d = 31$ design variables. In the theoretical model, each of these elements defining the geometry was divided into two subelements, giving a total of 60 finite elements. The optimal design problem defined by equations (14)–(16) involves finding the optimal values of the 31 beam nodal widths w_j subject to the stability constraints. The stability constraints were enforced only for the flow speed $U = 12{\cdot}8$ m/s, which turned out to be sufficient for the problems treated. In general, the stability constraints have to be enforced for some sub-critical speeds, to ensure that the structure is (theoretically) stable at the prescribed critical speed and all speeds below. The initial values $w_j = w_0$, corresponding to a uniform design, were chosen for solving the optimal design problem. The solution of the optimal design problem required approximately 25 iterations, giving a maximum residual in the design variables of less than 10^{-4} m.

The problem was solved for two different sets of lower bounds on the beam width, $\underline{w}_j = 0{\cdot}05$ m and $\underline{w}_j = 0{\cdot}03$ m. In the second case, the bounds on the tip variables $\underline{w}_{30}$ and $\underline{w}_{31}$ were set to 0·05 m for the attachment of the tip mass. The optimal design obtained by solving the optimal design problem is shown as Design 2 and 4 in Figure 3. Note that the design is based upon individual beam thickness, measured in the experimental tests (see Table 3). To experimentally verify the optimality of Design 2, a perturbed version, Design 3,

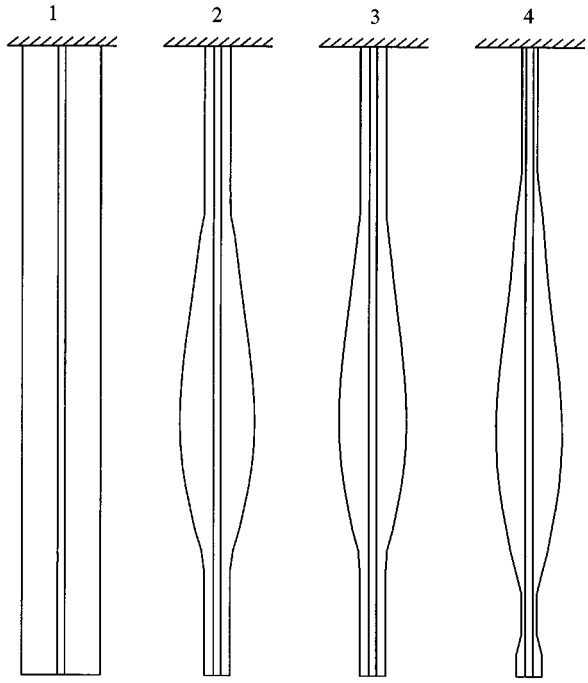

Figure 3. Investigated beams with fixed tip mass; the numbers on top refer to "Design 1", "Design 2," *et seq.*

TABLE 3
Comparison between theory and experiments for the investigated beams with fixed tip mass

Design	h (mm)	Mass ratio (%)	U^*_{pred} (m/s)	U_{pred} (m/s)	U_{exp} (m/s)	e_U (%)
1	2·80	100	10·7	12·8	12·2	4·8
2	2·92	57	10·1	12·8	12·9	0·8
3	2·92	53	10·0	12·3	12·4	0·8
4	2·99	49	9·2	12·8	13·7	6·8

was also investigated. The beam nodal widths of this design were simply 90% of the corresponding widths of Design 2, subject to the design constraints $\underline{w}_j = 0{\cdot}05$ m.

The experiments were performed with the approach described in Section 3.3. The results are compared with theoretical predictions in Table 3. Since only the beam structural mass is affected by the design, the ratio of the beam mass of the optimal design and the reference Design 1, is used as a measure of the design improvements. To investigate the design-dependence of the influence of damping, the predicted critical flow speed when damping is neglected, U^*_{pred}, is also presented.

Satisfactory agreement between numerical and experimental predictions was achieved in all tests. The optimality of Design 2 subject to the design constraints $\underline{w}_j = 0{\cdot}05$ m is clearly

indicated. Due to the local weakness of Design 4, it suffered from moderate static distortion when the speed was increased. The distortion tended to stabilize the structure, which is the most likely reason for the increase in critical speed compared to Design 2. Thus, the most optimal design exhibits a behaviour which is not predictable by the theory used for solving the optimal design problem. Damping is found to stabilize the same mode of instability for all cases, but the influence of damping is significantly design-dependent.

The deviations in flutter frequency was typically of the order 10–15%; however, for optimal Design 4, the deviation was 26%. The bifurcations appeared to be supercritical in all cases.

4.2. Optimal Design Without Tip Mass

The next optimal design problem stated, is to find the optimal width distribution of the beam without tip mass, such that the beam structural mass is minimized for the same critical flow speed as in the former case. By removing the tip mass and reducing the width of Design 1 by 37%, a new uniform design with the same critical speed $U_{\text{pred}} = 12{\cdot}8$ m/s is achieved. This design, shown as Design 5 in Figure 4, is the reference design in this section.

Using the same discretization and lower bounds on the beam width as in the previous case, the optimal designs shown as Designs 6 and 7 in Figure 4 are obtained by solving the optimal design problem. It is noted that Design 7 has a shape similar to optimized structures presented in Langthjem (1996) and Tanaka *et al.* (1993). A comparison to experimental tests is given in Table 4 in the same manner as before.

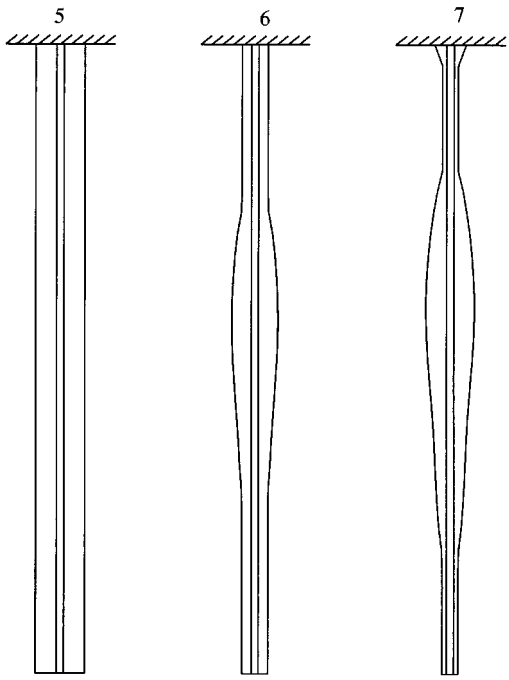

Figure 4. Investigated beams without tip mass.

TABLE 4
Comparison between theory and experiments for the investigated beams without tip mass

Design	h (mm)	Mass ratio (%)	U^*_{pred} (m/s)	U_{pred} (m/s)	U_{exp} (m/s)	e_U (%)
5	2·80	100	12·1	12·8	13·2	3·1
6	2·97	69	13·6	12·8	13·8	7·5
7	2·94	60	13·2	12·8	$>14{\cdot}3$	>11

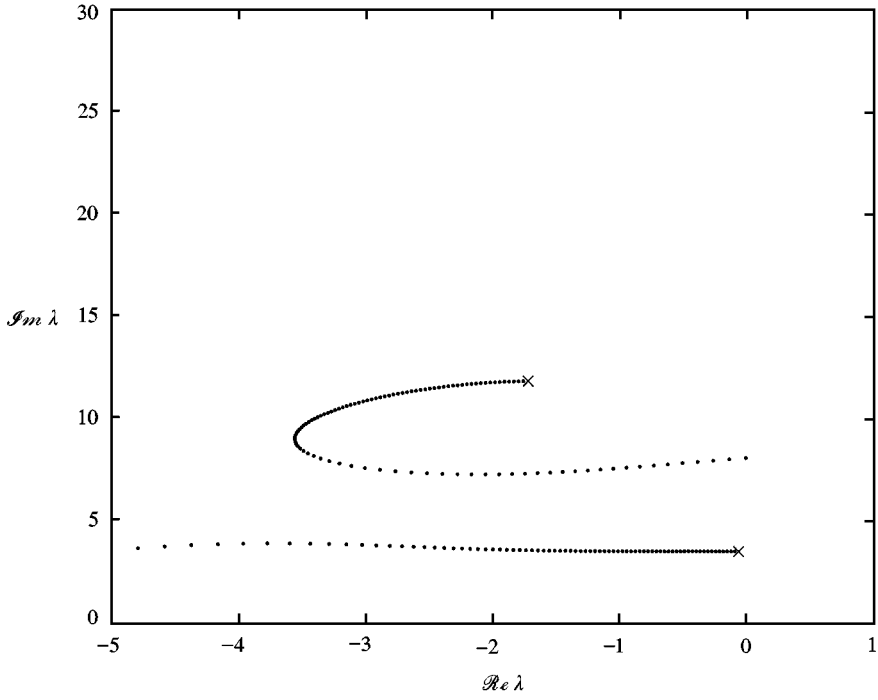

Figure 5. The root-locus plot of Design 6 with damping.

A sufficient accuracy was achieved for Designs 5 and 6, while Design 7 suffered from static distortion giving a deviation in critical speed larger than 11%. Unfortunately, the critical speed of Design 7 was larger than the maximum speed provided by the experimental set-up for the considered tube configuration, $U_{\max} = 14{\cdot}3$ m/s. Design 6 also suffered from moderate static distortion, which again tended to increase the critical speed. The same characteristics as in the former case were observed for the flutter frequencies and type of bifurcations.

An interesting feature of the optimal beams is that damping has a destabilizing effect (at least in theory). This may be explained by considering the root-locus plot of Design 6 for the cases with and without damping, see Figures 5 and 6. The root-locus plots are obtained by plotting the relevant eigenvalues from zero to critical flow speed. The eigenvalues corresponding to zero speed are marked by "$\times$". Obviously, the influence of damping causes

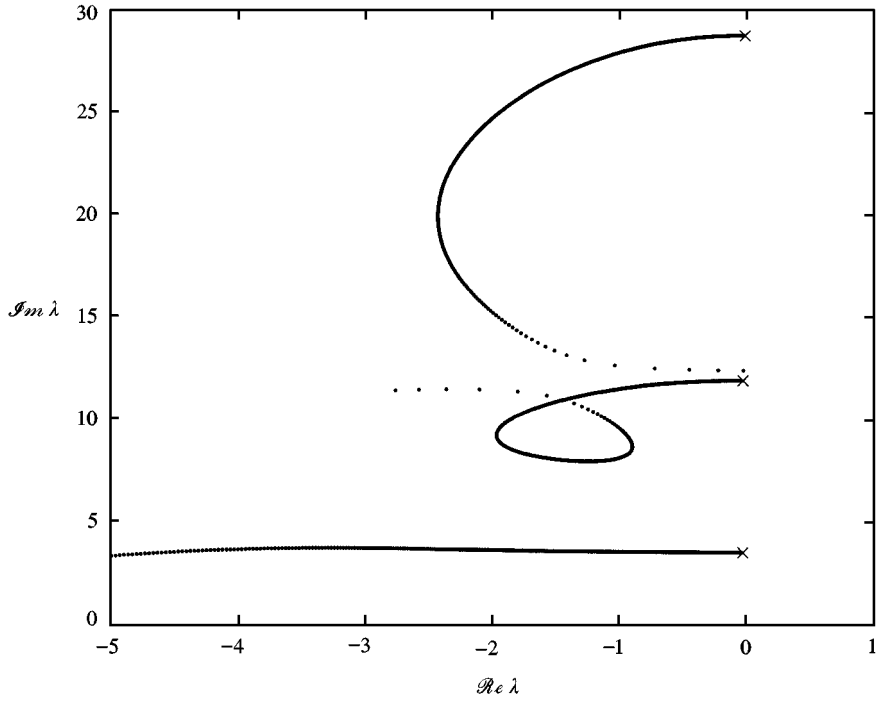

Figure 6. The root-locus plot of Design 6 without damping.

a shift in stability mode, making the system less stable. Using the full-damping model, all of the beams 1–7 become unstable in the same mode, and the root-locus plots look very much the same as in Figure 5.

4.3. Simultaneous Optimization of Beam and Tip Mass

Finally, the optimal design problem of finding the beam width distribution *and* the tip mass such that the total structural mass is minimized is solved. The problem formulation in Section 4.1 is extended to include a variable tip mass, giving a total of 32 design variables. By solving the optimal design problem, it is found that the optimal design has zero tip mass. Consequently, the beams in Section 4.2 are obtained, and the experimental investigation holds for this case too. The optimal Designs 6 and 7 give a total structural mass reduction of 45 and 48%, respectively.

5. CONCLUSIONS

The linear model based upon the plug-flow model for the fluid-dynamic forces and Euler–Bernoulli beam theory, accurately predicts the dynamic instability of the system investigated. The optimal design problem of minimizing the structural mass at constant critical flow speed was solved, and the numerical results were verified by experiments. Satisfactory accuracy was achieved provided that the optimal design problem was properly formulated by means of restricting the lower bound on the beam width. If sufficient care was

not taken, the optimal design suffered from static distortion due to the reduced beam stiffness, thus exhibiting a behaviour which cannot be predicted by the theory used for solving the optimal design problem. For the structures investigated, a reduction of the total structural mass up to approximately 50% was achieved. In this case, the possible improvement is limited by the presence of the tubes, which are not affected by the design process.

Structural damping was found to have a strong influence on the critical flow speed, and must be taken into account. It was also observed that the influence of damping on the critical speed was strongly design-dependent, which further necessitates the inclusion of damping in the model. This also means that the design is strongly affected by the amount of structural damping. With less structural damping, the optimal design would most likely be characterized by multiple bifurcations and/or shifts in the type of bifurcation (Langthjem 1996). This would further necessitate a proper formulation of the optimal design problem, in order to achieve the predicted performance in practice.

ACKNOWLEDGEMENTS

The author's supervisor, Professor Ulf Ringertz, is gratefully acknowledged for suggesting this most interesting topic of this project, and for much helpful advice. The author is indebted to Jakob Kuttenkeuler and Niklas Upphed for indispensable advice and help in experimental matters. He would also like to thank Dr Mikael Langthjem at the Technical University of Denmark for supplying tube material. The project was financially supported by the Swedish Research Council for Engineering Sciences (TFR).

References

Curtis, P. T. 1988 Crag test methods for the measurement of the engineering properties of fibre reinforced plastics. Technical Report 88012, Royal Aerospace Establishment, Farnborough, Great Britain.

Dowell, E. H., Curtiss, H. C. Scanlan, R. H. & Sisto, F. 1989 *A Modern Course in Aeroelasticity*. Dordrecht: Kluwer.

Haftka, R. T. & Adelman, H. M. 1993 Sensitivity of discrete systems. In *Optimization of Large Structural Systems* (ed. G. I. N. Rozvany), Vol. 1, pp. 289–311. Dordrecht: Kluwer.

Hill, J. L. & Swanson, C. P. 1970 Effects of lumped masses on the stability of fluid conveying tubes. *Journal of Applied Mechanics* **3,** 494–497.

Johnson, G. W. 1994 *LabVIEW Graphical Programming*. New York: McGraw-Hill.

Langthjem, M. A. 1996 Dynamics, stability and optimal design of structures with fluid interaction. Ph.D. Thesis, DCAMM Report S 71, Department of Solid Mechanics, The Technical University of Denmark.

Paidoussis, M. P. 1970 Dynamics of tubular cantilevers conveying fluid. *Journal of Mechanical Engineering Science* **12,** 85–103.

Paidoussis, M. P. & Li, G. X. 1993 Pipes conveying fluid: a model dynamical problem. *Journal of Fuids and Structures* **7,** 137–204.

Ringertz, U. T. 1994 On the design of Beck's column. *Structural Optimization* **8,** 120–124.

Sugiyama, Y., Matsuike, J., Ruy, B. J., Katayama, K., Kinoi, S. & Enomoto, N. 1995 Effect of concentrated mass on stability of cantilevers under rocket thrust. *AIAA Journal* **3,** 499–503.

Svanberg, K. 1993 The method of moving asymptotes (MMA) with some extensions. In *Optimization of Large Structural Systems*, (ed. G. I. N. Rozvany), Vol. 1, pp. 555–566. Dordrecht: Kluwer.

Tanaka, M., Tanaka, S. & Seguchi, Y. 1993 Optimal and robust shapes of a pipe conveying fluid. In *Proceedings of the Asia-Pacific Vibration Conference '93*, Vol. 4, pp. 1757–1762, JSME.